MATERIALS CHEMISTRY
FRONTIERS

RESEARCH ARTICLE

View Article Online
View Journal | View Issue

Cite this: *Mater. Chem. Front.*, 2019, **3**, 2437

Ultrasensitive detection of aqueous Cu^{2+} ions by a coumarin-salicylidene based AIEgen†

Subrata Kumar Padhan,[a] Narayan Murmu,[a] Subrat Mahapatra,[a] M. K. Dalai[b] and Satya Narayan Sahu*[a]

This work reports the aggregation induced emission (AIE) behaviour of a coumarin-salicylidene Schiff base probe **3** which shows bright yellow AIE fluorescence in DMSO–water medium (f_w 80%) buffered by 10 mM HEPES at pH 7.4. The aggregated probe (**AIEgen-3**) selectively discriminates Cu^{2+} ions over a series of other interfering metal ions *via* a fluorescence "on–off" strategy through a CHEQ process. DLS measurements revealed an average particle size of 372 nm for **AIEgen-3** at an 80% water fraction, which dramatically increases to 656 nm in the presence of Cu^{2+} ions, indicating the formation of more structured aggregates, which was further supported by TEM and ESI-MS experiments. A comprehensive analysis of the binding characteristics and interference studies of **AIEgen-3** with various metal ions have been carried out by fluorescence and UV-visible experiments. **AIEgen-3** shows a fluorescence detection limit (LOD) of 24 nM (~1.5 ppb) for Cu^{2+} ions, which is considerably far below the values of detection limits recently reported for other Cu^{2+} ion sensors in aqueous medium. Further, the analytical applications of **AIEgen-3** have been demonstrated by the estimation of Cu^{2+} ions in tap water and pharmaceutical samples both in solution and the solid phase, which shows the potentiality of the probe for on-site detection of Cu^{2+} ions in chemical, environmental and biological samples.

Received 17th June 2019,
Accepted 10th September 2019

DOI: 10.1039/c9qm00394k

rsc.li/frontiers-materials

1. Introduction

Recently the development of vibrant organic fluorophores possessing aggregation induced emission (AIE) characteristics in the aggregated/solid state is emerging as an important field of research due to their potential applications in organic light-emitting diodes (OLEDs), organic field-effect transistors (OFETs), solar cells, laser dyes, *etc.*[1–3] Further, AIE based probes have been meticulously employed for *in vivo* bioimaging applications and phototheranostic agents toward cancer cells.[4–7] In principle, those organic molecules which are weakly emissive in good solvents (mostly organic solvents) but exhibit strongly emissive behaviour in the presence of poor solvents (mostly water/buffers) due to molecular aggregation are referred to as AIE active fluorophores.[8–11] The mechanism behind the appearance of AIE properties in a molecular system is mainly attributed to restrictions in intramolecular rotation (RIR), intramolecular vibration (RIV) and/or intramolecular motion (RIM) within the molecule in the aggregated/solid state.[9,12] Moreover AIE active molecules possess unique advantages over classical aggregation caused quenching (ACQ) type fluorophores on account of their 'turn-on' fluorescence behavior on aggregation and facilitation of aggregation in highly aqueous medium/physiological conditions.[13,14] Therefore, AIE active fluorophores have been meticulously exploited for the development of chemo- and biosensors for monitoring vital analytes in chemical, environmental and biological samples in recent times.[15]

Amongst various analytes, the selective and sensitive detection of metal ions is highly desirable due to their important roles in many platforms. For instance, copper represents one of the important metals in industrial and domestic uses[16] and is considered as the third most abundant transition metal ion *in vivo*, playing a crucial role in the fundamental physiological processes of living organisms ranging from bacteria to mammals.[17,18] Further, copper ions are metabolically beneficial at optimal concentration, though can lead to serious health issues such as neurological disorders, and kidney and liver damage at higher concentrations.[18,19] According to the United States Environmental Protection Agency (USEPA) and World Health Organization (WHO), the maximum permissible limit for Cu^{2+} ions in drinking water should be within 15–25 μM,[20] beyond which they can cause cellular damage, and Alzheimer's and Wilson's diseases.[21,22] Therefore, development of analytical tools that can detect Cu^{2+} ions at micromolar concentrations with high selectivity and sensitivity in highly aqueous/physiological conditions is quite demanding.

[a] *School of Chemistry, Sambalpur University, Jyoti Vihar, Burla-768 019, Odisha, India. E-mail: snsahu.chem@gmail.com, snsahu@suniv.ac.in*
[b] *CSIR – Institute of Minerals & Materials Technology, Bhubaneswar - 751013, Odisha, India*

† Electronic supplementary information (ESI) available: UV-visible absorption, fluorescence and ESI-MS studies of probe **3** with Cu^{2+} ions. See DOI: 10.1039/c9qm00394k

In past years, Schiff bases have been reported as very good chelating ligands for binding of transition and heavy transition metal ions.[23,24] Besides, Schiff bases show excellent photophysical properties *via* excited-state intramolecular proton transfer (ESIPT), photochromism and thermochromism processes.[8,25,26] In recent studies, salicylidene based Schiff bases have emerged as potential molecules showing AIE characteristics in highly aqueous medium.[8,27] With this breakthrough, several salicylidene based Schiff bases possessing AIE properties have been developed as potential tools for the detection of Cu^{2+} ions (Table S1, ESI†).[28–35] The uniqueness of salicylidene based Schiff base molecules is the presence of phenolic 'O' and azomethine 'N', which can act as electron donors for binding metal ions. Thus, attachment of a chromogenic and/or fluorogenic moiety as a signalling subunit with the azomethine bond *via* π-conjugation could provide interesting optical responses during ion binding. Further, the chelating nature of ligands with metal ions strongly influences the fluorescence intensity of the metal–ligand complexes through modulating the energy levels of the ligand and metal ions. Accordingly, the binding of metal ions with the ligand may either ''turn-on'' or ''turn-off'' the original fluorescence signal of the ligand *via* chelation-enhanced fluorescence (CHEF) or chelation-enhanced quenching (CHEQ) processes, respectively. Fluorescence enhancement (CHEF) in metal–ligand complexes could be attributed to blocking of heteroatom (N/O/S) lone pair orbitals of the ligand through a stabilizing interaction with the vacant orbital of the metal centers, which possibly prevents the intramolecular photoinduced electron transfer (PET) phenomenon originating from the ligand lone pairs. In contrast, fluorescence quenching (CHEQ) could result from the electron/energy transfer from the ligand to the metal center (LMCT) *via* another PET pathway.[36] Therefore, it is envisaged that coumarin conjugated salicylidene derivatives can be exploited for the development of AIE based molecules which could trigger an optical output in the sensing medium upon interaction with metal ions.

With this vision and in continuation of our efforts toward the development of chromofluorescent metal ion sensors,[37,38] we have investigated the optical sensing behaviour of a coumarin-thiazolyl functionalized salicylidene Schiff base probe **3**. The probe demonstrates AIE properties in DMSO–water (buffered by 10 mM HEPES at pH 7.4) medium without undergoing hydrolytic cleavage of the azomethine linkage unlike other Schiff bases.[39] The aggregated probe **3** selectively interacts with Cu^{2+} ions through a visual fluorescent ''turn-off'' response in buffer medium at a physiological pH of 7.4 with a higher binding constant (K_a) and stronger Stern–Volmer constant (K_{SV}). Further, aggregated probe **3** shows a fluorescence detection limit (LOD) of 24 nM (~1.5 ppb) for Cu^{2+} ions, which is considerably far below the values of the LOD reported hitherto when compared with other Cu^{2+} ion sensors (Table S1, ESI†). In addition, the practical utility of the probe was analysed in tap water and commercially available copper ion containing pharmaceutical syrup (Lycopene) toward estimation of Cu^{2+} ions with more than 90% recovery. The solid state sensing of probe **3** for Cu^{2+} ions on a silica coated TLC plate additionally demonstrates its on-site applications for Cu^{2+} ion detection in various samples.

2. Experimental

2.1. Materials

All solvents and reagents (analytical grade and spectroscopic grade) were obtained from Merck (India) and Spectrochem Pvt. Limited (India) and were used without further purification. Probe **3** was synthesized according to Scheme 1 as per the procedure published in our previous work and characterised by using NMR, FTIR and mass spectroscopy (Fig. S1–S4, ESI†).[40] The AIE studies were carried out in DMSO–water (Milli-Q) buffered by 10 mM HEPES at pH 7.4 at varying DMSO–water fraction. In order to study the ionic interactions of probe **3**, metal ions such as Na^+, K^+, Ag^+, Al^{3+}, Ba^{2+}, Ca^{2+}, Cd^{2+}, Co^{2+}, Cr^{2+}, Cu^{2+}, Fe^{2+}, Hg^{2+}, Mg^{2+}, Mn^{2+}, Ni^{2+}, Pb^{2+}, Pd^{2+}, and Zn^{2+} in the form of their perchlorate/chloride/nitrate salts (10^{-3} to 10^{-4} M) dissolved in Milli-Q water were used. The binding studies of **3** were carried out in DMSO–water (Milli-Q) buffered by 10 mM HEPES at pH 7.4 at an 80% water fraction. 1 mM stock solution of probe **3** was prepared in UV-grade DMSO and subsequently used for preparation of lower concentrations of the probe solutions through appropriate dilution.

2.2. General methods

^{1}H NMR was recorded on an Avance III-400 MHz Bruker spectrometer. Chemical shifts are reported in parts per million from tetramethylsilane with the solvent (DMSO-d_6: 2.5 ppm) resonance as the internal standard. Data are reported as follows: chemical shifts, multiplicity (s = singlet, d = doublet, t = triplet, m = multiplet), coupling constant (Hz). UV-visible absorption spectra were recorded on a Shimadzu UV-2450 spectrophotometer. Fluorescence emission spectra were recorded on a Hitachi F-7000 fluorescence spectrophotometer. pH readings

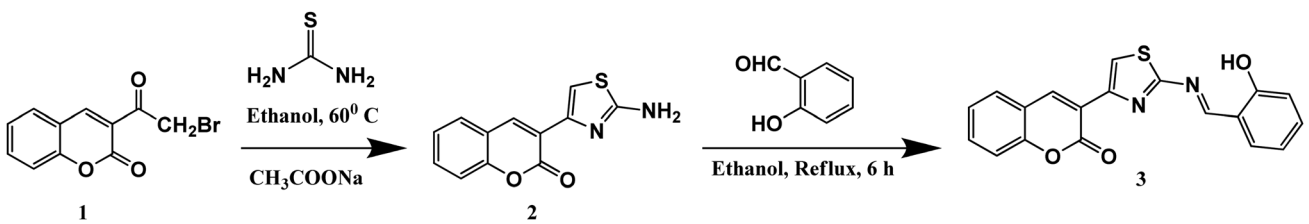

Scheme 1 Synthetic route for probe **3**.[40]

were measured using a UTECH CON-700 digital pH meter. Hydrodynamic diameters of the aggregates were measured using a Malvern Zetasizer instrument. Transmission electron microscopy (TEM) experiments were performed on an FEI Tecnai G^2 20 Twin instrument. HRMS experiments were performed on a Bruker ESI-MS microTOFQ instrument. Chromatographic purification was done using 60–120 mesh silica gels. For reaction monitoring, manually coated silica gel-300 mesh TLC plates were used.

2.3. Fluorescence and UV-visible studies of probe 3 with metal ions

For fluorescence and UV-visible experiments, a 50 μM concentration of probe **3** was prepared in DMSO–water (20 : 80 v/v) buffered by 10 mM HEPES at pH 7.4 from the 1 mM DMSO stock solution so as to form aggregates of the highest fluorescence intensities. The selectivity for metal ions was examined upon addition of 10.0 equivalents of various metal ions individually to 50 μM aggregated probe **3** buffered by 10 mM HEPES at pH 7.4. The corresponding emission spectra were recorded upon excitation of the aggregated probe **3** at 362 nm with a slit-width of 2.5 nm. Fluorescence and UV-visible titration experiments were carried out by gradual addition of various equivalents of Cu^{2+} ions through a micro pipette to a 2 mL (50 μM) solution of aggregated probe **3** in a 10 mm quartz cuvette.

2.4. Determination of the particle size by DLS measurements

The particle size measurements were carried out by DLS experiments taking probe **3** in different DMSO–water solutions (f_w 60%, 80%, and 99.5%) and in the presence of 2.0 equivalents of Cu^{2+} ions (at f_w 80%) by using a Malvern Zetasizer Instrument.

2.5. TEM analysis

The TEM measurements were carried out by taking **AIEgen-3** in DMSO–water solution (f_w 80%) in the absence and presence of 5.0 equivalents of Cu^{2+} ions.

2.6. ^{1}H NMR titration experiments

A 5 mM solution of probe **3** was prepared in DMSO-d_6. To 0.5 mL of the probe solution, various equivalents of copper perchlorate (from a stock of 10 mM in DMSO-d_6) were added in an NMR tube through a micro pipette and the spectra were recorded.

2.7. Calculation of the Stern–Volmer constant (K_{SV}) and limit of detection (LOD).

The extent of fluorescence quenching was calculated using the Stern–Volmer equation, eqn (1)[41]

$$\frac{I_0}{I} = 1 + K_{SV} \times [Cu^{2+}] \quad (1)$$

where K_{SV} represents the Stern–Volmer quenching constant, and I_0 and I respectively indicate the fluorescence intensities in the absence and presence of Cu^{2+} ions at various concentrations.

Similarly, the limit of detection (LOD) was calculated using eqn (2),

$$LOD = \frac{3\sigma}{K} \quad (2)$$

where σ and k respectively represent the standard deviation (for five measurements, n = 5) and slope of fluorescence intensity measured against various Cu^{2+} ion concentrations.

3. Results and discussion

3.1. Aggregation-induced emission (AIE) studies of probe 3

The aggregation induced emission characteristics of **3** were investigated at a 50 μM concentration in DMSO solution with addition of different fractions of water (f_w) ranging from 0 to 99.5% (v/v) buffered by 10 mM HEPES at pH 7.4. Fig. 1a presents the AIE character of **3** under a UV-lamp at 365 nm. The pure monomeric solution of **3** in 100% DMSO is almost colourless for visual detection. However, upon increasing the water fraction (buffered by 10 mM HEPES at pH 7.4), probe **3** emits yellow colour fluorescence beyond a 60% water fraction. In the fluorescence spectrum, probe **3** exhibits a weak emission band at 506 nm in 100% DMSO solution (50 μM) which decreases upon gradual addition of water and a new band at a longer wavelength of 544 nm appeared (Fig. 1b). The emission intensity at 544 nm corresponding to the yellow fluorescence of probe **3** increases from a 60% water fraction, exhibiting the highest intensity at 80% (f_w) (Fig. 1c). It was observed that addition of higher water fractions (f_w > 80%) results in reduction of the emission intensity. This is because at higher water fractions (f_w > 80%) probe **3** possibly forms larger molecular aggregates and precipitates quickly, resulting in a decrease in emission intensity, which is a characteristic phenomenon often observed with AIEgens.[42–46] Besides, dynamic light scattering (DLS) studies of probe **3** in different water fractions in DMSO (f_w 60%, 80% and 99.5%) also showed a decrease in the average particle size (Z_{av}) on addition of higher water volumes (Z_{av} at f_w 60% = 801 nm; at f_w 80% = 372 nm and at f_w 99.5% = 175 nm), indicating the formation of larger aggregates that precipitate out from the solution phase (Fig. S5, ESI†). However, the emission intensity at 544 nm for **3** is significantly increased 10 fold at an 80% water fraction, and even at a 99.5% water fraction, the fluorescence intensity is still much higher (~7 fold) than that in pure DMSO.

Interestingly, the Stokes shift in aggregated probe **3** at an 80% water fraction ($\Delta\lambda$ = 170 nm) is found to be much higher than that in pure DMSO ($\Delta\lambda$ = 132 nm), which is possibly because of the collective effect of ESIPT and AIE processes.[47,48] It is believed that, at lower water fractions (in good solvent conditions), the molecule (**3**) undergoes free rotation of the salicylidene aromatic unit around the C=N bond, resulting in suppression of ESIPT *via* non-radiative decay of excited states. However, as the volume of water increases beyond 60%, probe **3** suffers a restriction in its free rotation, possibly due to a decrease in solubility resulting from close packing/aggregation of the hydrophobic molecules through inter- and intra-molecular

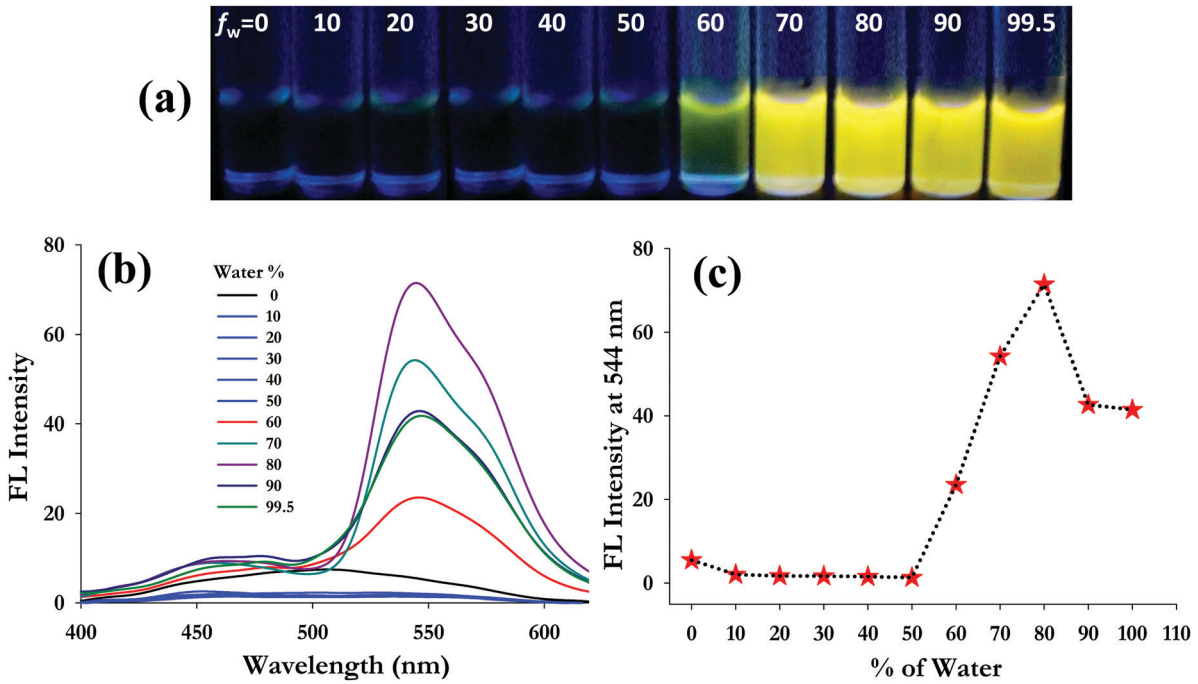

Fig. 1 (a) Visual fluorescence response of 50 μM probe **3** under a UV-lamp at 365 nm at varying DMSO–water (buffered by 10 mM HEPES at pH 7.4) fraction. (b) Fluorescence response for 50 μM probe **3** at varying DMSO–water (buffered by 10 mM HEPES at pH 7.4) fraction (λ_{ex} = 362 nm). (c) Change in the fluorescence intensity of probe **3** at 544 nm as a function of different percentages of the water fraction (% f_w).

hydrogen bonding. This restriction of intramolecular rotation (RIR) in aggregated probe **3** perhaps facilitates the radiative release of the photo-excited energy through suppression of non-radiative decay.[49] All the above findings clearly suggest that compound **3** is an AIE active fluorophore in poor solvent (aqueous) medium in which free intramolecular rotation of the fluorophore can be inhibited from the dispersed state to the aggregated state. For the investigation of metal ion interactions, the aggregated fluorophore **3** was taken in 20 : 80 (v/v) DMSO : HEPES buffer medium at pH 7.4, which is termed as **AIEgen-3** solution in subsequent discussion.

3.2. Fluorescence and UV-visible studies of AIEgen-3 with metal ions in HEPES buffer at pH 7.4

Fluorophore **3** comprises a π-conjugated framework possessing phenolic-OH and azomethine (>C═N–) linkages which are expected to bind metal ions. With this vision we have investigated the interaction of **AIEgen-3** with various metal ions. The fluorogenic response of **AIEgen-3** (50 μM) was investigated against 10 equivalents of various metal ions (such as Na^+, K^+, Ag^+, Al^{3+}, Ba^{2+}, Ca^{2+}, Cd^{2+}, Co^{2+}, Cr^{2+}, Cu^{2+}, Fe^{2+}, Hg^{2+}, Mg^{2+}, Mn^{2+}, Ni^{2+}, Pb^{2+}, Pd^{2+} and Zn^{2+} taken in HEPES buffered medium at pH 7.4) through visual fluorescence analysis under a UV-lamp at 365 nm. It was observed that **AIEgen-3** exhibited a diagnostic colour change from bright yellow fluorescence to non-fluorescent (colourless) only in the presence of Cu^{2+} ions, while no significant fluorescence response was observed in the presence of other metal ions under identical conditions (Fig. 2a).

Based on the results obtained from the visual fluorescence analysis, fluorescence and UV-visible spectroscopic investigations of **AIEgen-3** in the presence of 10 equivalents of various metal ions were performed. It was observed that addition of various metal ions to **AIEgen-3** solution quenched the aggregation induced emission band at 544 nm only in the presence of Cu^{2+} ions (Fig. 2b). The competitive metal ion interaction of **AIEgen-3** in the presence of 10 equivalents of various metal ions was also examined individually upon addition of 10 equivalents of Cu^{2+} ions and is depicted in Fig. 2c. This clearly demonstrates that the fluorescence intensity of **AIEgen-3** at 544 nm gets completely quenched by Cu^{2+} ions even in the presence of other interfering metal ions. This result indicates a very high level of selectivity of **AIEgen-3** toward Cu^{2+} ions. The selectivity behaviour was again monitored by UV-visible spectroscopy by addition of various metal ions to the **AIEgen-3** solution (50 μM). The results indicated that the absorption maximum at 374 nm significantly decreases in the presence of Cu^{2+} ions, while other metal ions could not produce any detectable change in its UV-visible spectrum (Fig. S6, ESI†). Further, a comparative absorbance study at 374 nm for **AIEgen-3** in the presence of various metal ions showed a significant decrease in the absorption intensity only in the presence of Cu^{2+} ions, which indicates a high level of selectivity of the probe toward Cu^{2+} ions (inset of Fig. S6, ESI†).

In order to understand the binding characteristics of **AIEgen-3** with Cu^{2+} ions, a fluorescence titration experiment was performed by gradual addition of a standard solution of Cu^{2+} ions to a 50 μM **AIEgen-3** solution which resulted in a progressive decrease of the emission intensity centred at 544 nm (Fig. 3a). A detail analysis of the fluorescence titration profile indicated that the decrease in fluorescence intensity is initiated by the addition of 0.2 equivalents and saturation

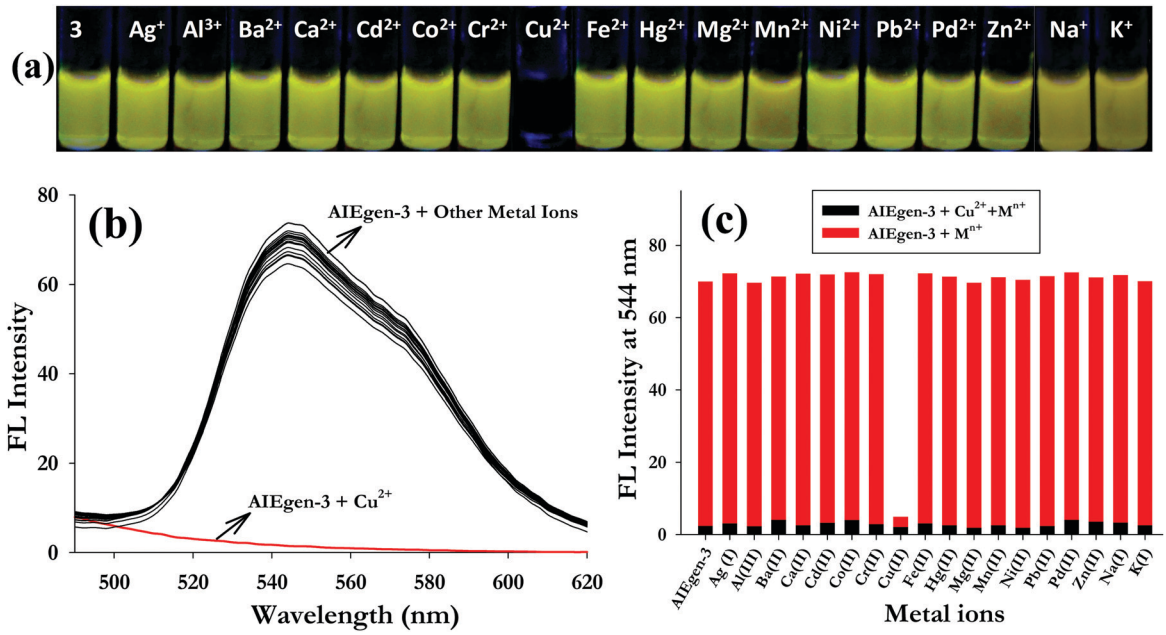

Fig. 2 (a) Visual fluorescence response under a UV-lamp at 365 nm; (b) emission spectra of **AIEgen-3** (50 μM) upon addition of 10 equiv. of various metal ions; (c) histogram showing the fluorescent intensity of **AIEgen-3** at 544 nm with 10 equiv. of various metal ions (red bars) and with 10 equiv. of various metal ions plus 10 equiv. of Cu^{2+} ions (black bars) [λ_{ex} = 362 nm].

begins after the addition of 1.0 equivalent of Cu^{2+} ions (inset of Fig. 3a). The fluorescence intensity was quenched almost by 16% upon addition of only 0.2 equiv. of Cu^{2+} ions to the **AIEgen-3** solution and over 90% quenching was observed by the addition of 1.0 equiv. of copper ions. The quenching of the fluorescence signal in **AIEgen-3** by Cu^{2+} ions may be attributed to the paramagnetic nature of this ion, which results in chelation-enhanced quenching (CHEQ) possibly *via* a ligand to metal charge transfer process between the copper ions and **AIEgen-3**.[50] Moreover, to understand the extent and nature of fluorescence quenching in **AIEgen-3** by Cu^{2+} ions, the Stern–Volmer plot was analysed. A linear relationship for the Stern–Volmer plot was obtained for Cu^{2+} ions with a correlation coefficient (R^2) equal to 0.98 and a quenching constant (K_{SV}) value of $3.89 \times 10^4\ M^{-1}$ as obtained from the slope of the linear plot (Fig. 3b). The higher K_{SV} value clearly indicates a significantly stronger interaction between **AIEgen-3** and copper ions, which quench the fluorescence signal possibly *via* a static mechanism.[51]

The apparent association constant (K_a) was determined from nonlinear regression analysis of the fluorescence signal at 544 nm against various equivalents of Cu^{2+} ions using Sigma-scientific data analysis software (inset of Fig. 3a) and was found to be $1.67 \times 10^5\ M^{-1}$. Similarly, the UV-visible titration profile of **AIEgen-3** with Cu^{2+} ions follows a parallel trend to that of the fluorescence titration with a decrease in the absorption intensity at 450 nm through addition of Cu^{2+} ions (Fig. S7, ESI†). The association constant (K_a) was determined from the absorption intensity at 450 nm against various equivalents of Cu^{2+} ions by nonlinear regression analysis (inset of Fig. S7, ESI†) and was found to be $2.4 \times 10^5\ M^{-1}$. The association constant value obtained from fluorescence measurements shows good agreement with the same obtained from UV-visible spectroscopy measurements. These findings clearly indicate a very high binding affinity of **AIEgen-3** toward Cu^{2+} ions.

3.3. Determination of the binding stoichiometry and limit of detection (LOD) of AIEgen-3 with Cu^{2+} ions

The binding stoichiometry of **AIEgen-3** with Cu^{2+} ions was quantitatively analysed by a fluorescence method using a Job continuous variation plot, which revealed a deviation point at a 0.5 mol fraction of the probe, indicating a 1 : 1 binding stoichiometry between **AIEgen-3** and Cu^{2+} ions (Fig. S8, ESI†). This observation is in accordance with the respective fluorescence and UV-visible titration profiles, indicating good correlation of the binding stoichiometry. The sensitivity of **AIEgen-3** has been evaluated further by determining the limit of detection (LOD) from the fluorescence measurement at 544 nm at a 10 μM concentration of **AIEgen-3** upon addition of Cu^{2+} ions. The LOD for **AIEgen-3** was found to be 24 nM (~1.5 ppb) (Fig. S8, ESI†), which is considerably lower than the other Cu^{2+} ion sensors published so far (compared in Table S1, ESI†).[28–35] This value is markedly far below the permissible level of Cu^{2+} ions (about 15–25 μM) in drinking water as recommended by the USEPA and WHO,[20] indicating that **AIEgen-3** can be employed as a suitable candidate for ultrasensitive detection of Cu^{2+} ions in real water samples. The time response of **AIEgen-3** for Cu^{2+} ions was also studied as a function of time by monitoring changes in the fluorescence intensity at 544 nm in DMSO : HEPES buffer (2 : 8 v/v at pH 7.4) medium. It was observed that Cu^{2+} ions interact with **AIEgen-3** within 6 minutes, resulting in complete quenching of the fluorescence signal (Fig. S9, ESI†).

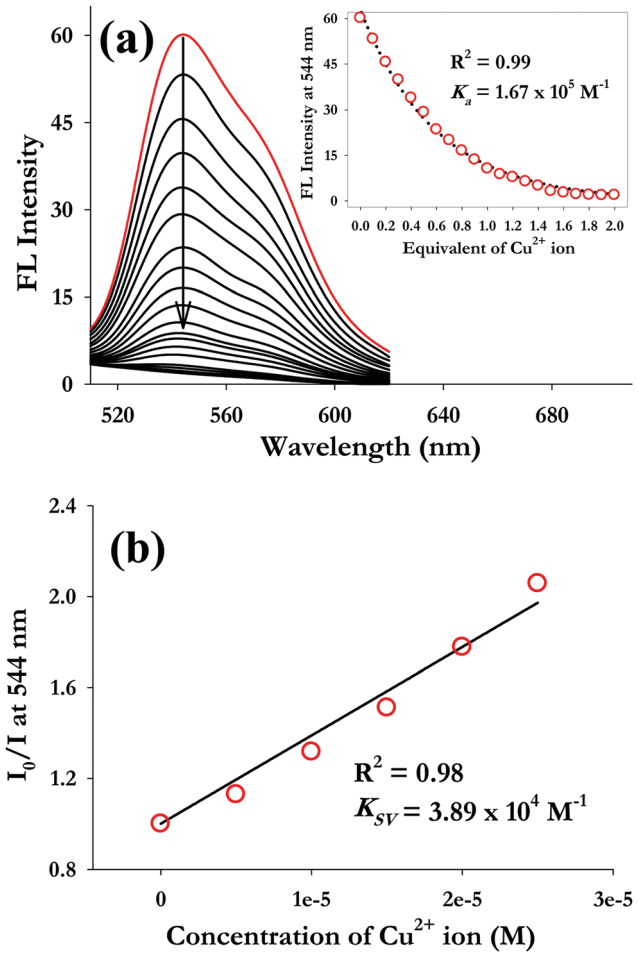

Fig. 3 (a) Fluorescence titration spectra of **AIEgen-3** upon addition of 0 to 2.0 equiv. of Cu^{2+} ions. Inset shows the change in fluorescence intensity at 544 nm against various equiv. of Cu^{2+} ions. (b) Stern–Volmer plot for **AIEgen-3** in the presence of various concentrations of Cu^{2+} ions [λ_{ex} = 362 nm].

3.4. Effect of pH on AIEgen-3 and its interaction with Cu^{2+} ions in aqueous medium

The effect of pH on the emissive response of **AIEgen-3** and its binding behaviour toward Cu^{2+} ions was also investigated by taking a series of pH solutions ranging from 1 to 13 in aqueous medium (Fig. 4). From the fluorescence measurements it was observed that **AIEgen-3** is quite stable within the pH range of 5–9. However, below pH 5 and above pH 9, the emission intensity of **AIEgen-3** is altered, possibly because of protonation and deprotonation of the phenolic OH group, respectively, in a highly acidic and basic pH medium. This process may disrupt the OH–N=C< intramolecular hydrogen bonding, which is a key factor for the origin of AIE.

Protonation or deprotonation creates ionic charge over the molecule and thereby increases the solubility of the probe, which may dissociate the aggregates, resulting in the loss of the AIE band. Based on these findings we have examined the optical response of **AIEgen-3** toward Cu^{2+} ions in the pH range of 5–9 by fluorescence analysis in aqueous medium (Fig. 4). Addition of 10.0 equivalents of Cu^{2+} ion to **AIEgen-3** resulted in

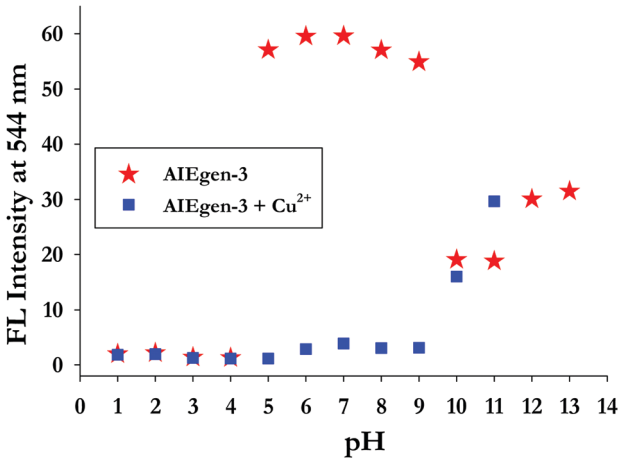

Fig. 4 Effect of pH on the emission intensities of **AIEgen-3** (50 μM) at 544 nm in the absence (red stars) and in the presence (blue squares) of 10 equiv. of Cu^{2+} ions [λ_{ex} = 362 nm].

a change in fluorescence colour from bright yellow to colourless (non-emissive) with a significant quenching in its emission band at 544 nm over the tested pH range. This observation further validates the application of **AIEgen-3** for the fluorogenic detection of Cu^{2+} ions over a wide pH range of 5–9.

3.5. Mechanism of interaction of Cu^{2+} with AIEgen-3

The mechanism of interaction of probe **3** with copper ions has also been studied by dynamic light scattering (DLS), transmission electron microscopy (TEM) and ESI-mass spectrometry (ESI-MS) experiments. For instance, the aggregation behavior of probe **3** in poor solvent (water) in the absence and presence of Cu^{2+} ions has been examined from particle size measurements by DLS experiments. The results showed that the average particle size (Z_{av}) of **AIEgen-3** (f_w 80%) in the absence of copper ions is estimated to be 372 nm (Fig. S5, ESI†). However, in the presence of 2.0 equivalents of Cu^{2+} ions the average particle size dramatically increases to 656 nm (Fig. S5, ESI†), which indicated an obvious effect of Cu^{2+} ions on the aggregation pattern of the probe. Further, the morphology of **AIEgen-3** aggregates has been investigated by TEM analysis, which clearly indicates the formation of discrete aggregated nanoparticles in the range of 300–400 nm (Fig. 5a). The addition of Cu^{2+} ions to **AIEgen-3** modulates the aggregation pattern of the probe, which results in the formation of pinnate leaf type aggregates (Fig. 5b). Moreover, the formation of the **AIEgen-3**–Cu^{2+} complex

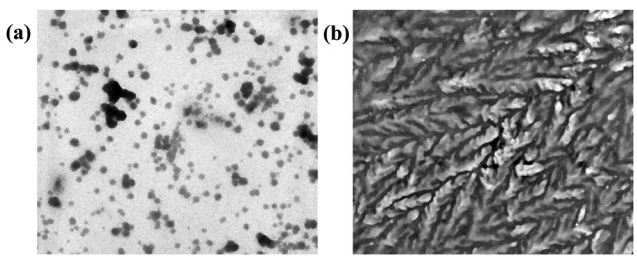

Fig. 5 TEM micrograph of (a) **AIEgen-3** and (b) **AIEgen-3** + Cu^{2+}.

was also analysed by ESI-MS, which showed a strong peak at *m*/*z* 245.03 which could be attributed to the dimeric complex $[2(\text{AIEgen-3})\cdot 2\text{Cu}\cdot \text{ClO}_4\cdot \text{CH}_3\text{CN}\cdot \text{H}_2\text{O}\cdot \text{H}]^{4+}$ (calculated *m*/*z* 245.24) (Scheme 2 and Fig. S10, ESI†).

All these findings clearly suggest that the aggregated **AIEgen-3** interacts with Cu^{2+} ions resulting in swelling of the aggregates *via* copper ion intercalation leading to the formation of larger particles. The aggregated copper complex possibly quenches the AIE fluorescence signal of **AIEgen-3** at 544 nm *via* a Cu^{2+} mediated PET mechanism. A proposed binding model and sensing mechanism of **AIEgen-3** with Cu^{2+} ions is depicted in Scheme 2.

Finally, the fluorescence recovery of **AIEgen-3** through decomplexation of Cu^{2+} ions by various molecular competitors such as EDTA, ethylenediamine, hydrazine, and aniline and anionic competitors such as S^{2-}, CN^-, F^-, Cl^-, Br^-, I^-, $H_2PO_4^-$, and HSO_4^- has been evaluated. Surprisingly, no significant recovery of the fluorescence signal at 544 nm was observed even after the addition of an excess of the above competitive species. This observation clearly indicated the formation of a significantly tight complex between **AIEgen-3** and Cu^{2+} ions, possibly due to their higher binding affinity. Further, the aggregated self-assembly network of the [**AIEgen-3**–Cu^{2+}] complex is expected to be stable enough *via* aromatic π–π stacking and hydrogen bonding interactions.[34]

3.6. ^{1}H NMR titration of probe 3 in the presence of various equivalents of Cu^{2+} ions

The binding characteristics of probe **3** with Cu^{2+} ions were also investigated by ^{1}H NMR titration experiments in DMSO-d_6. Fig. 6 presents the ^{1}H NMR titration spectra of **3** in the absence and presence of various equivalents of Cu^{2+} ions. The proton signals H5, H6 and H7 showed downfield shifts upon gradual addition of Cu^{2+} ions, which clearly indicates the interaction of azomethine-N, thiazoly-N and coumarin-C(O) atoms respectively with Cu^{2+} ions during complex formation. On the other hand, there is an upfield shift observed in the aromatic proton signals that could be attributed to an increase of charge density within the probe complex that promotes intramolecular charge transfer in the probe.[52] As a result, the aggregates accumulated more Cu^{2+} ions and formed larger and tighter aggregate complexes. Thus the comparatively rigid planar structure of **3** will be bent in the presence of Cu^{2+} ions and the new aggregates resulted in strong chelation-enhanced fluorescence quenching (CHEQ).[34] The aggregate structural changes and sensing mechanism have been depicted in Scheme 2.

3.7. On-site applications of AIEgen-3 for detection of Cu^{2+} ions in the solid state

In order to examine the on-site utility of probe **3**, we have evaluated the optical behavior of **3** on manually coated silica gel TLC plates in the presence of Cu^{2+} ions. The TLC test plates were prepared by spotting with a 1 mM acetonitrile solution of probe **3** and left until dry, which gives an aggregated form of **AIEgen-3** in the solid state. Then various concentrations of Cu^{2+} ions (ranging from 0.1 to 1000 μM) were prepared in water medium and 10 μL of each sample was spotted in the middle of the previously coated probe and visualized under a UV-lamp at 365 nm.

It was observed that addition of Cu^{2+} ions significantly quenched the yellow fluorescence of probe **3** in the solid state (black spots within the yellow spots), which can be distinctly visible and detectable up to a 1 μM concentration of Cu^{2+} ions (Fig. 7a) indicating thereby the high sensitivity of this probe toward copper ions. These findings signified that probe coated

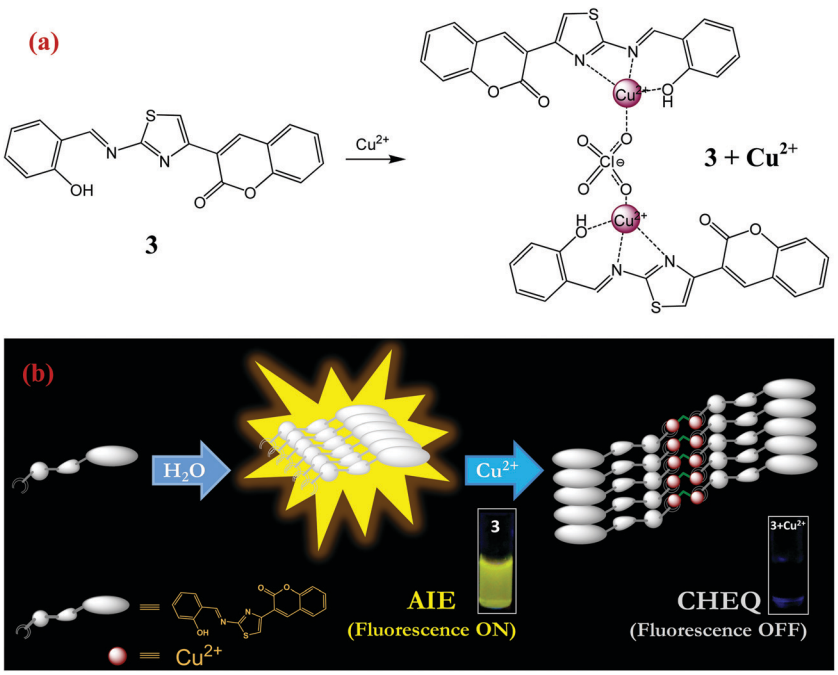

Scheme 2 (a) Proposed binding model and (b) sensing mechanism of **AIEgen-3** with Cu^{2+} ions.

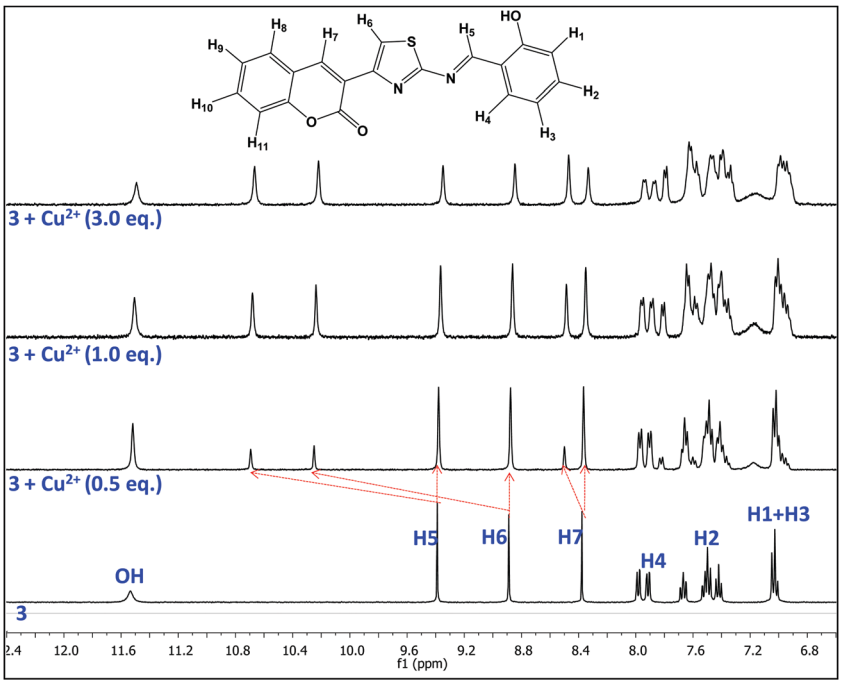

Fig. 6 ^{1}H NMR titration spectra of probe **3** (5.0 mM) with various equiv. of Cu^{2+} ions in DMSO-d_6.

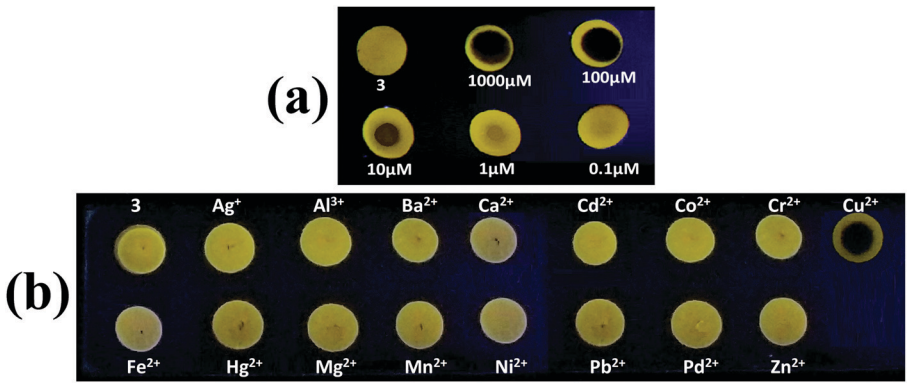

Fig. 7 (a) Visual optical response of probe **3** for various conc. of Cu^{2+} ions; (b) selectivity toward 10 μL of various metal ions (50 μM in water medium) under a UV-lamp at 365 nm in the solid state spotted on a TLC plate.

plates can be employed for the direct detection of Cu^{2+} ions at the very low concentrations present in environmental samples. In addition, the selectivity of probe **3** was also investigated in the solid state by spotting 10 μL solutions of various metal ions (50 μM in water medium) in the middle of the previously coated TLC plate with probe **3** and viewing under a UV-lamp at 365 nm. Interestingly, a black spot within the yellow spots (fluorescence quenching) was observed only in the case of Cu^{2+} ions, while other metal ions could not produce any diagnostic optical change in the probe yellow spots (Fig. 7b). This result evidently demonstrated that the probe is extremely selective for detection of Cu^{2+} ions even in the solid state.

3.8. Analytical applications

Considering the importance of monitoring Cu^{2+} ions in environmental samples, the detection and estimation of copper ions by **AIEgen-3** has been investigated in the natural environment by fluorescence measurements. In order to verify the possible interference of other components and ions present in real samples during detection of Cu^{2+} ions, we have taken town supply tap water as the medium of analysis. The extent of fluorescence quenching in **AIEgen-3** (50 μM) with known concentrations of Cu^{2+} ions has been calibrated and found to be in excellent linear correlation (R^2 = 0.99) over the range 5 μM to 50 μM (Fig. S11, ESI†). Now solutions of Cu^{2+} ions in varying concentrations were prepared in tap water and estimated using the calibration plot (Fig. S11, ESI†). The results obtained from these experiments are summarized in Table 1, which indicated that **AIEgen-3** could be applied for the detection and estimation of Cu^{2+} ions in environmental samples. In addition, **AIEgen-3** is also capable of estimating the amount of Cu^{2+} ions present in a pharmaceutical syrup sample (Lycopene syrup) without any

Table 1 Estimation of Cu^{2+} ions by **AIEgen-3** in real samples using fluorescence assay

Sample	Cu^{2+} added (μM)	F.I. at 544 nm (a.u.)	Cu^{2+} found (μM)	RSD[a] (%)	Estimation (%)
AIEgen-3 (50 μM) (blank)	0	59.85	—	—	—
Tap water sample-1	5	52.47	4.69	1.25	93.8
Tap water sample-2	10	46.31	9.58	1.31	95.8
Lycopene syrup-1	—	47.63	8.67	1.62	—
Lycopene syrup-2	5	43.47	12.44	1.19	91.0

[a] RSD (%) = percent relative standard deviation.

pretreatment of the syrup solution. This will definitely open up new opportunities to estimate Cu^{2+} ions directly in pharmaceutical formulations.

4. Conclusions

In summary, a chromofluorescent salicylidene Schiff base **3** functionalized with a thiazolyl-coumarin derivative has been investigated for optical detection of metal ions. Probe **3** shows aggregation induced emission (AIE) characteristics at different water fractions in DMSO medium to elicit bright yellow fluorescence under UV-illumination at 365 nm. The aggregated probe **AIEgen-3** selectively discriminates Cu^{2+} ions over a series of other interfering metal ions by a fluorescence ''on–off'' strategy *via* a CHEQ process in DMSO–HEPES buffer (2 : 8 v/v) at a physiological pH of 7.4. DLS measurements revealed a particle size of 372 nm for **AIEgen-3** at an 80% water fraction, which dramatically increases to 656 nm in the presence of Cu^{2+} ions, indicating the formation of more structured aggregates. Moreover, ESI-MS studies revealed the formation of a dimeric copper complex with **AIEgen-3**, which was further supported by TEM analysis. Job plot analysis revealed a 1 : 1 binding stoichiometry between **AIEgen-3** and Cu^{2+} ions. Further, **AIEgen-3** is fairly stable over a wide pH range of 5 to 9 and interacts with Cu^{2+} ions selectively through visual fluorescent ''turn-off'' behaviour in buffer medium at a physiological pH of 7.4. The higher binding constant ($K_a = 1.67 \times 10^5\ M^{-1}$), stronger Stern–Volmer constant ($K_{SV} = 3.89 \times 10^4\ M^{-1}$) and a very low limit of detection (LOD) of 24 nM concentration indicates the ultra sensitivity of **AIEgen-3** toward Cu^{2+} ions. In addition the practical utility of the probe was analysed in tap water and commercially available copper ion containing pharmaceutical syrup (Lycopene) toward estimation of Cu^{2+} ions with more than 90% recovery. Moreover, the solid state sensing of **AIEgen-3** for Cu^{2+} ions on a silica coated TLC plate indicates the potentiality of the probe for on-site detection of Cu^{2+} ions in chemical, environmental and biological samples.

Conflicts of interest

The authors declare no competing financial interest.

Acknowledgements

S. N. S. gratefully acknowledges the financial assistance received from DST, New Delhi, Govt. of India, for the Fast-Track project grant (SR/FT/CS-46/2011) and S&T Department, Govt. of Odisha for the research grant. The research grant received from GNM Foundation for the Prof. GN Mahapatra Endowment Chair award is gratefully acknowledged. S. K. P. is thankful to DST and UGC New Delhi for a project assistantship and BSR fellowship respectively. N. M. is grateful to S&T Department, Govt. of Odisha for a project fellowship. The authors are thankful to Central Instruments Facility, NIT Rourkela for recording the NMR spectra. A special thanks to Prof. Parameswar Krishnan Iyer and Mr Niranjan Meher of IIT Guwahati for carrying out the DLS experiments reported in this paper. We thank Mr Ajit Dash, CSIR-IMMT, Bhubaneswar for carrying out the TEM experiments reported in this work. The financial assistance received from UGC and DST New Delhi under the DRS and FIST grant respectively to the School of Chemistry is gratefully acknowledged. We are thankful to Dr H. Chakraborty, Sambalpur University and Dr Chandra Shekhar Purohit, NISER, Bhubaneswar for their useful suggestions toward the improvement of this manuscript.

References

1 H. Nie, J. Huang, Z. Zhao and B. Z. Tang, Aggregation-Induced Emission Luminogens (AIEgens) for Non-Doped Organic Light-Emitting Diodes, *Aggregation-Induced Emission: Materials and Applications*, 2016, ch. 7, vol. 2, pp. 173–198.
2 J. Deng, Y. Xu, L. Liu, C. Feng, J. Tang, Y. Gao, Y. Wang, B. Yang, P. Lu, W. Yang and Y. Ma, An ambipolar organic field-effect transistor based on an AIE-active single crystal with a high mobility level of 2.0 $cm^2\ V^{-1}\ s^{-1}$, *Chem. Commun.*, 2016, **52**, 2370–2373.
3 G. Feng, R. T. K. Kwok, B. Z. Tang and B. Liu, Functionality and versatility of aggregation-induced emission luminogens, *Appl. Phys. Rev.*, 2017, **4**, 021307.
4 H. Gao, X. Zhang, C. Chen, K. Li and D. Ding, Unity Makes Strength: How Aggregation-Induced Emission Luminogens Advance the Biomedical Field, *Adv. Biosyst.*, 2018, **2**, 1800074.
5 J. Qi, C. Chen, X. Zhang, X. Hu, S. Ji, R. T. K. Kwok, J. W. Y. Lam, D. Ding and B. Z. Tang, Light-driven transformable optical agent with adaptive functions for boosting cancer surgery outcomes, *Nat. Commun.*, 2018, **9**, 1848.
6 C. Chen, H. Ou, R. Liu and D. Ding, Regulating the Photophysical Property of Organic/Polymer Optical Agents for Promoted Cancer Phototheranostics, *Adv. Mater.*, 2019, **31**, 1806331.
7 X. Ni, X. Zhang, X. Duan, H.-L. Zheng, X.-S. Xue and D. Ding, Near-Infrared Afterglow Luminescent Aggregation-Induced

Emission Dots with Ultrahigh Tumor-to-Liver Signal Ratio for Promoted Image-Guided Cancer Surgery, *Nano Lett.*, 2019, **19**, 318–330.

8 J. Mei, N. L. C. Leung, R. T. K. Kwok, J. W. Y. Lam and B. Z. Tang, Aggregation-Induced Emission: Together We Shine, United We Soar!, *Chem. Rev.*, 2015, **115**, 11718–11940.

9 Y. Hong, J. W. Y. Lama and B. Z. Tang, Aggregation-induced emission: phenomenon, mechanism and applications, *Chem. Commun.*, 2009, 4332–4353.

10 Y. Hong, J. W. Y. Lam and B. Z. Tang, Aggregation-induced emission, *Chem. Soc. Rev.*, 2011, **40**, 5361–5388.

11 J. Mei, Y. N. Hong, J. W. Y. Lam, Y. H. Tang and B. Z. Tang, Aggregation-Induced Emission: The Whole Is More Brilliant than the Parts, *Adv. Mater.*, 2014, **26**, 5429–5479.

12 H. Qian, M. E. Cousins, E. H. Horak, A. Wakefield, M. D. Liptak and I. Aprahamian, Suppression of Kasha's rule as a mechanism for fluorescent molecular rotors and aggregation-induced emission, *Nat. Chem.*, 2017, **9**, 83–87.

13 C. Zhan, X. You, G. Zhang and D. Zhang, Bio-/Chemosensors and Imaging with Aggregation-Induced Emission Luminogens, *Chem. Rec.*, 2016, **16**, 2142–2160.

14 L. Mao, Y. Liu, S. Yang, Y. Li, X. Zhang and Y. Wei, Recent advances and progress of fluorescent bio-/chemosensors based on aggregation-induced emission molecules, *Dyes Pigm.*, 2019, **162**, 611–623.

15 D. D. La, S. V. Bhosale, L. A. Jones and S. V. Bhosale, Tetraphenylethylene-Based AIE-Active Probes for Sensing Applications, *ACS Appl. Mater. Interfaces*, 2018, **10**, 12189–12216.

16 V. K. Gupta, I. Ali and H. Y. Aboul-Enein, Metal ions speciation in the environment: distribution, toxicities and analyses, *Developments in Environmental Science*, 2007, ch. 3, vol. 5, pp. 33–56.

17 H. Kozlowski, A. Janicka-Klos, J. Brasun, E. Gaggelli, D. Valensin and G. Valensin, Copper, iron, and zinc ions homeostasis and their role in neurodegenerative disorders (metal uptake, transport, distribution and regulation), *Coord. Chem. Rev.*, 2009, **253**, 2665–2685.

18 B. Ashish, K. Neeti and K. Himanshu, Copper Toxicity: A Comprehensive Study, *Res. J. Recent Sci.*, 2013, **2**, 58–67.

19 E. L. Que, D. W. Domaille and C. J. Chang, Metals in Neurobiology: Probing Their Chemistry and Biology with Molecular Imaging, *Chem. Rev.*, 2008, **108**, 1517–1549.

20 M. Kumar and A. Puri, A review of permissible limits of drinking water, *Indian J. Occup. Environ. Med.*, 2012, **16**, 40–44.

21 E. Gaggelli, H. Kozlowski, D. Valensin and G. Valensin, Copper Homeostasis and Neurodegenerative Disorders (Alzheimer's, Prion, and Parkinson's Diseases and Amyotrophic Lateral Sclerosis), *Chem. Rev.*, 2006, **106**, 1995–2044.

22 S. Lutsenko, A. Gupta, J. L. Burkhead and V. Zuzel, Cellular multitasking: The dual role of human Cu-ATPases in cofactor delivery and intracellular copper balance, *Arch. Biochem. Biophys.*, 2008, **476**, 22–32.

23 C. J. Dhanaraj, J. Johnson, J. Joseph and R. S. Joseyphus, Quinoxaline-based Schiff base transition metal complexes: review, *J. Coord. Chem.*, 2013, **66**, 1416–1450.

24 G. Yuan, H. Jiang, L. Zhang, Y. Liu and Y. Cui, Metallosalen-based crystalline porous materials: Synthesis and property, *Coord. Chem. Rev.*, 2019, **378**, 483–499.

25 V. S. Padalkar and S. Seki, Excited state intramolecular proton transfer (ESIPT) inspired solid state emitters, *Chem. Soc. Rev.*, 2016, **45**, 169–202.

26 E. Hadjoudis and I. M. Mavridis, Photochromism and thermochromism of Schiff bases in the solid state: structural aspects, *Chem. Soc. Rev.*, 2004, **33**, 579–588.

27 W. Tang, Y. Xiang and A. Tong, Salicylaldehyde Azines as Fluorophores of Aggregation-Induced Emission Enhancement Characteristics, *J. Org. Chem.*, 2009, **74**, 2163–2166.

28 M. A. Assiria, A. G. Al-Sehemia and M. Pannipara, AIE based "on-off" fluorescence probe for the detection of Cu^{2+} ions in aqueous media, *Inorg. Chem. Commun.*, 2019, **99**, 11–15.

29 N. Miengmern, A. Koonwong, S. Sriyab, A. Suramitrc, R. P. Pooarpornd, S. Hannongbua and S. Suramitr, Aggregation-induced emission enhancement (AIEE) of N,N′-Bis(Salicylidene)-*p*-Phenylenediamine Schiff base: Synthesis, photophysical properties and its DFT studies, *J. Lumin.*, 2019, **210**, 493–500.

30 R. Yadav, A. Rai, A. K. Sonkar, V. Rai, S. C. Gupta and L. Mishra, A viscochromic, mechanochromic, unsymmetrical azine for selective detection of Al^{3+} and Cu^{2+} ions and its mitotracking studies, *New J. Chem.*, 2019, **43**, 7109–7119.

31 J. Yang, J. Chai, B. Yang and B. Liu, Achieving highly sensitive detection of Cu^{2+} based on AIE and FRET strategy in aqueous solution, *Spectrochim. Acta, Part A*, 2019, **211**, 272–279.

32 H. Liu, R. Wei, Y. Xiang and A. Tong, Fluorescence turn-on detection of pyrophosphate based on aggregation induced emission property of 5-chlorosalicylaldehyde azine, *Anal. Methods*, 2015, **7**, 753–758.

33 K. Tiwari, S. Kumar, V. Kumar, J. Kaur, S. Arora and R. K. Mahajan, An azine based sensor for selective detection of Cu^{2+} ions and its copper complex for sensing of phosphate ions in physiological conditions and in living cells, *Spectrochim. Acta, Part A*, 2018, **191**, 16–26.

34 B. Liu, H. Zhou, B. Yang and X. Hu, Aggregation–induced emission activity and further Cu^{2+} induced self-assembly process of two Schiff compounds, *Sens. Actuators, B*, 2017, **246**, 554–562.

35 H. Zhou, B. Yang, G. Wen, X. Hu and B. Liu, Assembly and disassembly activity of two AIEE model compounds and its potential application, *Talanta*, 2018, **184**, 394–403.

36 A. T. Afaneh and G. Schreckenbach, Fluorescence Enhancement/Quenching Based on Metal Orbital Control: Computational studies of a 6-Thienyllumazine-Based mercury sensor, *J. Phys. Chem. A*, 2015, **119**, 8106–8116.

37 S. K. Padhan, J. Palei, P. Rana, N. Murmu and S. N. Sahu, Sequential displacement strategy for selective and highly sensitive detection of Zn^{2+}, Hg^{2+} and S^{2-} ions: an approach toward a molecular keypad lock, *Spectrochim. Acta, Part A*, 2019, **208**, 271–284.

38 S. K. Padhan, P. Rana, N. Murmu, B. S. Swain and S. N. Sahu, Solvent modulated optical tuning for discrimination of Hg^{2+}, Zn^{2+} and Cu^{2+} ions by a coumarin-functionalized

azine receptor, *Indian J. Chem., Sect. B: Org. Chem. Incl. Med. Chem.*, 2019, **58**, 167–182.

39 B. Pramanik and D. Das, Aggregation Induced Emission or Hydrolysis by Water? The Case of Schiff Bases in Aqueous Organic Solvents, *J. Phys. Chem. C*, 2018, **122**, 3625–3661.

40 S. K. Padhan, M. B. Podh, P. K. Sahu and S. N. Sahu, Optical discrimination of fluoride and cyanide ions by coumarin-salicylidene based chromofluorescent probes in organic and aqueous medium, *Sens. Actuators, B*, 2018, **255**, 1376–1390.

41 J. R. Lakowicz, *Principles of Fluorescence Spectroscopy*, Springer, New York, 3rd edn, 2006.

42 R. Suresh, S. K. Thiyagarajan and P. Ramamurthy, An AIE based fluorescent probe for digital lifting of latent finger-print marks down to minutiae level, *Sens. Actuators, B*, 2018, **258**, 184–192.

43 M. Shyamal, S. Maity, A. Maity, R. Maity, S. Roy and A. Misra, Aggregation induced emission based "turn-off" fluorescent chemosensor for selective and swift sensing of mercury(II) ions in water, *Sens. Actuators, B*, 2018, **263**, 347–359.

44 M. Shyamal, P. Mazumdar, S. Maity, S. Samanta, G. P. Sahoo and A. Misra, Highly Selective Turn-On Fluorogenic Chemosensor for Robust Quantification of Zn(II) Based on Aggregation Induced Emission Enhancement Feature, *ACS Sens.*, 2016, **1**(6), 739–747.

45 B. Liu, Y. Y. Bao, H. Wang, F. F. Du, J. Tian, Q. B. Li, T. S. Wang and R. K. Bai, An efficient conjugated polymer sensor based on the aggregation-induced fluorescence quenching mechanism for the specific detection of palladium and platinum ions, *J. Mater. Chem.*, 2012, **22**, 3555–3561.

46 M. Shyamal, P. Mazumdar, S. Maity, G. P. Sahoo, G. Salgado-Moran and A. Misra, Highly Selective Turn-On Fluorogenic Chemosensor for Robust Quantification of Zn(II) Based on Aggregation Induced Emission Enhancement Feature, *J. Phys. Chem. A*, 2016, **120**, 210–220.

47 A. S. Gupta, K. Paul and V. Luxam, A fluorescent probe with "AIE + ESIPT" characteristics for Cu^{2+} and F^{-} ions estimation, *Sens. Actuators, B*, 2017, **246**, 653–661.

48 D. Xua, M. Liua, H. Zoua, J. Tiana, H. Huanga, Q. Wana, Y. Daia, Y. Wena, X. Zhanga and Y. Wei, A new strategy for fabrication of water dispersible and biodegradable fluorescent organic nanoparticles with AIE and ESIPT characteristics and their utilization for bioimaging, *Talanta*, 2017, **174**, 803–808.

49 T. Han, Y. Hong, N. Xie, S. Chen, N. Zhao, E. Zhao, J. W. Y. Lam, H. H. Y. Sung, Y. Dong, B. Tong and B. Z. Tang, Defect-sensitive crystals based on diaminomaleonitrile-functionalized Schiff base with aggregation-enhanced emission, *J. Mater. Chem. C*, 2013, **1**, 7314–7320.

50 P. N. Borase, P. B. Thale and G. S. Shankarling, Dihydroquinazolinone based "turn-off" fluorescence sensor for detection of Cu^{2+} ions, *Dyes Pigm.*, 2016, **134**, 276–284.

51 M. Pannipara, A. G. Al-Sehemi, A. Kalam, A. M. Asiri and M. N. Arshad, AIE active turn-off fluorescent probe for the detection of Cu^{2+} ions, *Spectrochim. Acta, Part A*, 2017, **183**, 84–89.

52 S. S. Razi, P. Srivastava, R. Ali, R. C. Gupta, S. K. Dwivedi and A. Misra, A coumarin-derived useful scaffold exhibiting Cu^{2+} induced fluorescence quenching and fluoride sensing (On–Off–On) via copper displacement approach, *Sens. Actuators, B*, 2015, **209**, 162–171.